MucosalImmunology

www.nature.com/mi

ARTICLE

IRF4-dependent dendritic cells regulate CD8$^+$ T-cell differentiation and memory responses in influenza infection

Erola Ainsua-Enrich[1], Ibrahim Hatipoglu[1], Sapana Kadel[1,2], Sean Turner[1], Jinny Paul[1], Simar Singh[1], Harini Bagavant[1] and Susan Kovats[1,2]

Acute respiratory disease caused by influenza viruses is imperfectly mitigated by annual vaccination to select strains. Development of vaccines that elicit lung-resident memory CD8$^+$ T cells (T_{RM}) would offer more universal protection to seasonal and emerging pandemic viruses. Understanding how lung-resident dendritic cells (DCs) regulate T_{RM} differentiation would be an important step in this process. Here, we used CD11c-cre-*Irf4*$^{f/f}$ (KO) mice, which lack lung-resident IRF4-dependent CD11b$^+$CD24^{hi} DCs and show IRF4 deficiency in other lung cDC subsets, to determine if IRF4-expressing DCs regulate CD8$^+$ memory precursor cells and T_{RM} during influenza A virus (IAV) infection. KO mice showed defective CD8$^+$ T-cell memory, stemming from a deficit of T regulatory cells and memory precursor cells with decreased *Foxo1* expression. Transfer of wild-type CD11b$^+$CD24^{hi} DCs into KO mice restored CD8$^+$ memory precursor cell numbers to wild-type levels. KO mice recovered from a primary infection harbored reduced numbers of CD8$^+$ T_{RM} and showed deficient expansion of IFNγ$^+$CD8$^+$ T cells and increased lung pathology upon challenge with heterosubtypic IAV. Thus, vaccination strategies that harness the function of IRF4-dependent DCs could promote the differentiation of CD8$^+$ T_{RM} during IAV infection.

Mucosal Immunology (2019) 12:1025–1037; https://doi.org/10.1038/s41385-019-0173-1

INTRODUCTION

Influenza virus infection results in acute respiratory disease and elicits innate immunity, neutralizing antibodies and cytotoxic effector and memory T cells.[1] Antiviral responses eliminate infected cells but may result in excess inflammation and immune-mediated pathology that prolong illness.[2] While current influenza vaccines elicit antibodies to strain-specific glycoproteins, vaccination strategies that promote differentiation and retention of memory T cells recognizing conserved internal proteins will enhance universal protection to seasonal and emerging pandemic viruses.[3,4] Optimal responses of lung-resident dendritic cells (DCs) will be a key component of such vaccine strategies.[5]

Lung-resident DCs, acting in the lung or after migration to mediastinal lymph nodes (mLN), coordinate immune responses to respiratory viruses. Migratory DCs include CD103$^+$CD11b$^-$CD24^{hi} (CD103$^+$) DCs and two subsets of CD11b$^+$SIRPα$^+$CD103$^-$ DCs distinguished as CD24^{hi}CD11b$^+$ (CD11b$^+$P1) or CD24^{int}CD11b$^+$ (CD11b$^+$P2).[6,7] The transcription factors IRF8 and BATF3 control CD103$^+$ DC differentiation, while IRF4 is required for the development of CD11b$^+$P1 lung DCs.[6–9] Analogous subsets of IRF4$^+$CD1c$^+$ and IRF8$^+$CD141$^+$ DCs are present in human respiratory tissue.[7,10] Monocyte-derived "inflammatory" CD11b$^+$ DCs (iDCs) also accumulate in the lung and mLN after respiratory infection.[11,12] Functional roles of lung-resident DCs and iDCs during respiratory virus infection have been defined.[11–18] In *Batf3*$^{-/-}$ mice, the absence of CD103$^+$ DCs leads to decreased numbers of protective CD8$^+$ T cells during respiratory virus infection including IAV,[8,19] consistent with their cross-presentation of viral antigens and early production of IL-12.[8,17,20] CD11b$^+$ DCs, including CCR2$^+$ iDCs, express IL-12p70 and CD70 promoting T_H1 and CD8$^+$ T-cell expansion.[11,15] However, the difficulty in distinguishing inflammatory and resident CD11b$^+$ DCs with shared markers has hampered definition of how lung-resident CD11b$^+$P1 and CD11b$^+$P2 DCs regulate T cells during IAV infection. *CD11c-cre-Irf4*$^{f/f}$ mice provide an opportunity to resolve this issue.[6] In homeostasis, *CD11c-cre-Irf4*$^{f/f}$ mice lack the IRF4-dependent lung-resident CD11b$^+$P1 DCs, while CD11b$^+$P2 and CD103$^+$ DC subsets are present in normal numbers but lack IRF4.[6] A distinct *CD11c-cre-Irf4*$^{f/f}$ model, in which a different CD11c-cre construct does not lead to absence of the CD11b$^+$P1 DCs, did not show defects in T-cell responses in primary IAV infection, and T memory responses were not studied.[21]

Viral infection results in circulating CD62L^{hi}CCR7^{hi} central memory T cells (T_{CM}) and CD62L^{lo}CCR7^{lo} effector memory T cells (T_{EM}) and extravascular CD69$^+$CD103$^+$ resident memory T cells (T_{RM}) retained in peripheral tissues.[22,23] After IAV infection, lung T_{RM} cells contribute to protection against heterosubtypic viruses in mice, although they wane over time in the lower respiratory tract.[4,24–27] T_{RM} also have been identified in human lungs.[28,29] The role of distinct DC subsets in formation of memory T cells during IAV infection is not completely understood. Prior reports showed that CD11b$^+$ DCs support differentiation of CD8$^+$ T_{CM} cells,[19] while CD103$^+$ DCs promote optimal CD8$^+$ T_{RM} priming but not subsequent T_{RM} differentiation or circulating memory T cells.[30] Collaboration between functionally unique DC subsets may regulate an optimal balance of CD8$^+$ T effector and memory populations by influencing the differentiation of late effector subsets. In LCMV infection, abundant IL-12 favors IL-7Rα^{lo}KLRG1$^+$T-BET^{hi} short-lived effector

[1]Arthritis & Clinical Immunology Program, Oklahoma Medical Research Foundation, Oklahoma City, OK 73104, USA and [2]Department of Microbiology and Immunology, University of Oklahoma Health Sciences Center, Oklahoma City, OK 73104, USA
Correspondence: Susan Kovats (Susan-Kovats@omrf.org)

Received: 31 August 2018 Revised: 23 April 2019 Accepted: 27 April 2019
Published online: 15 May 2019

cells (SLECs), and IL-10 promotes IL-7Rα^{hi}KLRG1^{-}T-BET^{lo} memory precursor effector cells (MPECs).[31] Upon infection resolution, the pool of SLECs contracts, while MPECs convert to memory T cells by upregulating FOXO1.[31–33] T regulatory cell (T_{REG}) production of IL-10 promotes CD8^{+} memory T cells during LCMV infection,[34] but the role of DCs in the regulation of induced T_{REGs} or MPECs during IAV infection is less well understood.[35,36] IRF4 in DCs promotes transcription of *Il10*[21], and inhibits IL-12,[37] suggesting that IRF4 regulates the balance of IL-12 and IL-10.

Herein, we report that during IAV infection, *CD11c-cre-Irf4$^{f/f}$* mice showed increased numbers of IAV-specific IFNγ^{+}CD8^{+} effector T cells but a marked deficit in FOXP3^{+} T_{REGs} and CD8^{+} MPECs. Recovered *CD11c-cre-Irf4$^{f/f}$* mice harbored lower numbers of lung CD8^{+} T_{EM} and T_{RM} cells, and upon exposure to heterosubtypic IAV, showed reduced expansion of IAV-specific IFNγ^{+}TNFα^{+}CD8^{+} T cells, which correlated with increased lung damage. Thus, IRF4-expressing lung-resident DCs promote the differentiation of CD8^{+} memory T cells during IAV infection.

RESULTS

CD11c-cre-Irf4$^{f/f}$ mice contain greater numbers of influenza antigen-specific CD4^{+} and CD8^{+} IFNγ^{+} T cells in the mediastinal LN after IAV infection

To determine the role of IRF4-dependent DCs during IAV infection, we infected *CD11c-cre-Irf4$^{+/+}$* (WT) and *CD11c-cre-Irf4$^{f/f}$* (KO) mice intranasally with a sublethal dose of A/Puerto Rico/8/1934 (PR8) virus. We monitored daily weight loss as a sign of morbidity and the kinetics of virus clearance, but we did not identify significant reproducible differences in these parameters between WT and KO mice (Fig. 1a, Fig. S1a). However, by day 12 post infection (p.i.), the KO mice showed significantly increased (1.7-fold) numbers of mLN cells (Fig. 1b) and tended to have more CD45.2^{+} cells in the lung compared to the WT mice (Fig. 1c), suggesting a greater immune response to virus.

To determine if CD4^{+} and CD8^{+} IAV antigen-specific T cells expanded more in KO mice during the infection, we measured numbers of CD4^{+} and CD8^{+} nucleoprotein (NP)-specific T cells in the mLN using H-2D^{b}/NP366-374 and I-A^{b}/NP311-325 tetramers on days 8, 10 and 12 p.i. Although numbers of tetramer-positive (Tet^{+}) CD4^{+} and CD8^{+} T cells in WT and KO mice were similar on days 8–10 p.i., the numbers of Tet^{+}CD8^{+} T cells in WT had contracted while the numbers in KO mice remained ~2-fold elevated on 12 p.i. (Fig. 1d). Similarly, on day 12 p.i., numbers of Tet^{+}CD4^{+} T cells were higher in KO mice (Fig. 1e). To determine if antigen-specific T cells in WT and KO differed in functional capacity, mLN cells were isolated on day 12 p.i. and activated ex vivo with IAV-specific peptides: I-A^{b}-binding NP311-325 and H-2D^{b}-binding NP366-374 (Fig. S2a). While antigen-specific WT and KO CD4^{+} and CD8^{+} T cells produced comparable amounts of IFNγ as judged by mean fluorescence intensity (MFI) (Fig. S1b) and the fraction (frequency of live cells) of mLN CD8^{+} or CD4^{+} mLN T cells producing IFNγ was not different (Fig. S1c), KO mice harbored significantly increased (1.7−2-fold) numbers of antigen-specific CD8^{+} and CD4^{+} IFNγ^{+} T cells (Fig. 1f, g). This is consistent with elevated IFNγ in the bronchoalveolar lavage fluid of KO mice compared to WT mice (Fig. S1d). However, numbers of NP-specific CD8^{+} and CD4^{+} T cells capable of producing IFNγ in the lung on day 12 p.i. did not differ in WT and KO mice (Fig. S1e). These data show that KO mice expand greater numbers of CD4^{+} and CD8^{+} effector T cells in the mLN during IAV infection.

CD11c^{+} lung DCs in CD11c-cre-Irf4$^{f/f}$ mice show decreased IL-10 and increased IL-12a RNA levels during IAV infection

Upon IAV infection, the lung-resident CD103^{+} and CD11b^{+} DCs acquire and present viral antigens, produce cytokines including IL-12 and IL-10 and migrate to the draining mLN where they elicit an adaptive immune T-cell response leading to production of IFNγ.[1] Migratory CD103^{+} DCs are a significant source of IL-12 at early time points post infection by intracellular pathogens, while IRF4-expressing CD11b^{+} DCs may be a primary source of IL-10.[20,21] In infected WT mice, the CD11b^{+} and CD103^{+} lung-resident migratory DC subsets express distinct levels of IRF4 in the lung and mLN, with the highest level in CD11b^{+}P1 DCs (Fig. 2a; Fig. S2b). To determine if IRF4 deficiency might alter the balance of DC-produced IL-12 and IL-10, total CD11c^{+} cells from the lung were isolated day 3 p.i. and assayed for *Il10* and *Il12a* RNA by qPCR. In the KO mice, CD11c^{+} lung cells expressed significantly lower (1.8-fold) levels of *Il10* and tended to express higher levels of *Il12a* (Fig. 2b).

To identify the DC subsets synthesizing *Il10*, *Il12a* and *Il12b* RNA, we sorted lung DC subsets on day 5 p.i. CD11c^{+}MHCII^{+}Ly6C^{-}CD88^{-} lung-resident DCs were sorted as CD103^{+}CD11b^{-} (CD103^{+}), CD103^{-}CD11b^{+}SIRPα^{+}CD24^{hi} (CD11b^{+}P1) and CD103^{-}CD11b^{+}SIRPα^{+}CD24^{int} (CD11b^{+}P2); all three subsets were CD64^{-} (Fig. S2b). We also sorted CD11b^{+}Ly6C^{hi} iDCs that accumulate by day 5 p.i.; for KO mice, we sorted the ~50% of iDCs that were GFP^{+}, indicating *Irf4* deletion. WT CD11b^{+} P1 and P2 DCs contained *Il-10* RNA (Fig. 2c), although this RNA was not detectable in all WT mice, perhaps due to the kinetics of infection varying in individual mice. At early time points, some DCs have migrated from the lung to the mLN, and the number of activated (IL-10 or IL-12a producing) DCs remaining in each lung may vary. Ly6C^{hi} iDCs also contained *Il-10* RNA, and these levels were reduced in IRF4$^{-/-}$ GFP^{+} iDCs in some KO mice (Fig. 2c). Among WT DCs, *Il12a* RNA was detectable in Ly6C^{hi} iDCs, while all DC subsets contained *Il12b* RNA (Fig. 2c). Notably, *Il12a* RNA was elevated ~17-fold in KO CD103^{+} DCs (Fig. 2c). Thus, the absence of the CD11b^{+}P1 DCs and *Irf4*-deficiency in other DC subsets led to decreased *Il10* and increased *Il12a* RNA in DCs.

CD11c-cre-Irf4$^{f/f}$ mice show quantitative and qualitative defects in CD8^{+} memory precursor T cells during the resolution phase of infection

IL-12 induces the expression of the transcription factor T-BET in T cells, thus promoting the differentiation of IFNγ-producing effector T cells.[31] Consistent with elevated *Il12a* and reduced *Il10* RNA in KO DCs, KO mice have increased (~1.8-fold) numbers of CD44^{hi} CD8^{+} and CD4^{+} T cells expressing T-BET compared to WT mice in the lung on day 5 p.i. (Fig. 3a; Fig. S3a, b). On day 5 p.i., we detected very few Tet^{+} T cells, and it was difficult to determine if they had higher levels of T-BET in KO mice. T-BET^{+} T-cell numbers (either Tet^{+} or the total pool) were similar in WT and KO mice days 6 and 8 p.i. (Fig. 3a), suggesting distinct kinetics in WT and KO mice. Depending on the expression level of T-BET, CD8^{+} T cells differentiate into SLEC and MPEC subsets of late effectors as determined by IL-7Rα and KLRG1 expression (Fig. 3b; Fig. S3c).[31] By day 10 p.i., KO mice showed a significant reduction (1.9-fold) in numbers of antigen-specific (Tet^{+}) IL-7Rα^{+}KLRG1^{-} MPECs in the lung (Fig. 3c; Fig. S3c). However, numbers of Tet^{+}IL-7Rα^{-} KLRG1^{+} SLECS did not differ in WT and KO lungs (Fig. 3d).

To determine if the MPECs in KO mice show an altered transcriptional program, we sorted CD8^{+}Tet^{+} MPECs (GFP^{-}) from WT and KO lungs on day 10 p.i. and assayed expression of selected genes important for memory T-cell differentiation (Fig. 3e, f). KO MPECS contained reduced (1.7-fold) levels of *Foxo1* RNA, a transcription factor that regulates the program of memory T cells (Fig. 3e).[38,39] RNA levels of the FOXO1-regulated transcription factors *Bcl6* and *Eomes*, which promote the development of MPECs to memory CD8^{+} T cells, also were reduced (2−2.8-fold) in KO MPECs (Fig. 3e). RNA levels of genes involved in CD8^{+} T-cell effector function (*Tbx21, Prdm1, Id2*) and survival (*Bcl2, Bcl2l11, Noxa*), tissue residence of T_{RM} (*Klf2, S1pr1*), or regulation of memory (*Foxo3*) were not different in WT and KO MPECs (Fig. 3f; Fig. S3d−f). Taken together, these data suggest that the absence

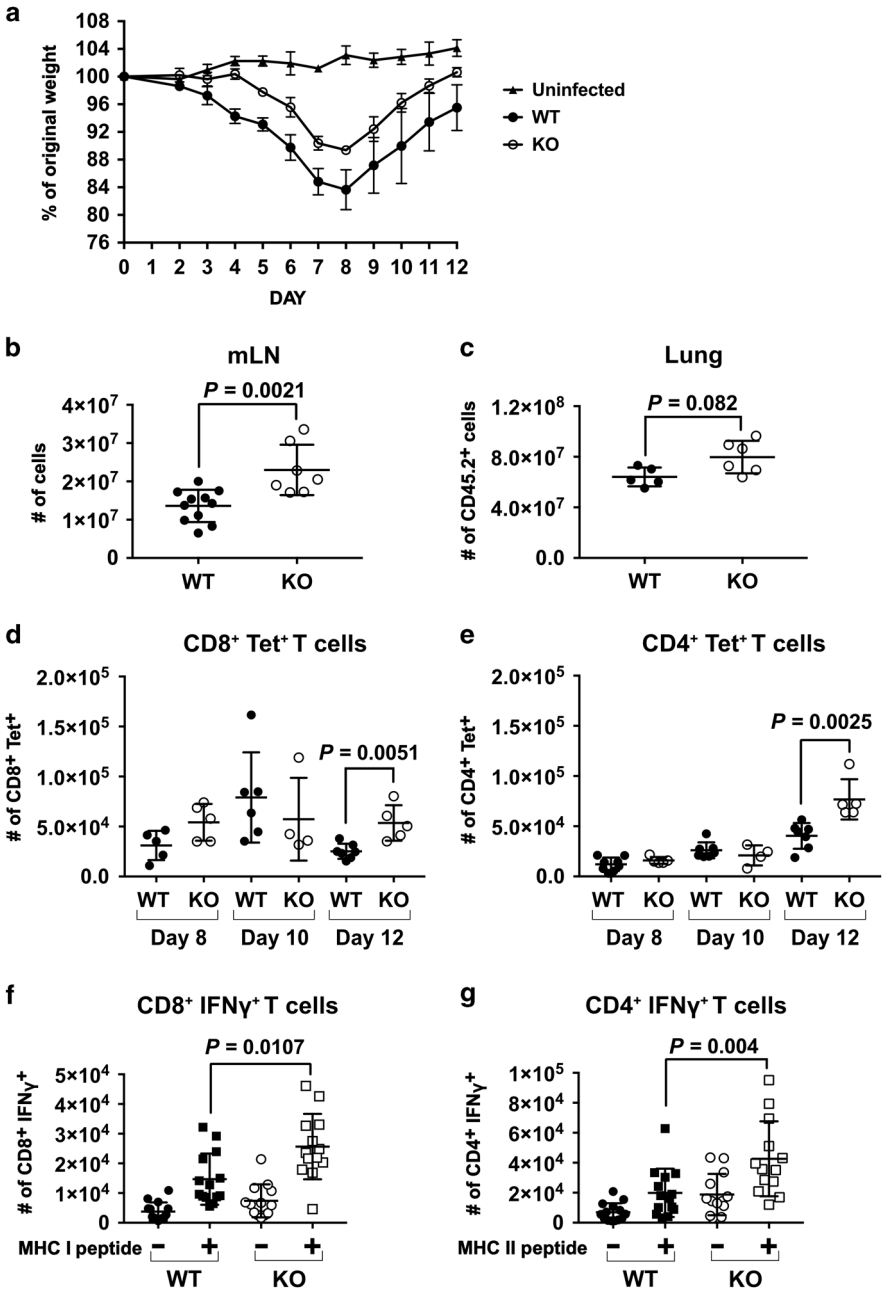

Fig. 1 *CD11c-cre-Irf4$^{f/f}$* mice harbor higher numbers of antigen-specific CD4$^+$ and CD8$^+$ IFNγ$^+$ T cells in the mLN after IAV infection. WT and KO mice were infected i.n. with a sublethal dose of PR8 IAV. **a** Weight loss and recovery of WT and KO mice ($n = 3$ each) over 12 days p.i. with PR8 virus. Shown are the mean and SEM. Differences in WT and KO mice were not significant as determined by a multiple *t* test with the Bonferroni−Sidak method. **b** Total numbers of mLN cells on day 12 p.i. **c** Total numbers of CD45$^+$ cells in the lung on day 12 p.i. **d** Numbers of CD8$^+$ T cells binding H-2D^b/NP366-374 tetramers (Tet) and **e** numbers of CD4$^+$ T cells binding I-A^b/NP311-325 tetramers in the mLN on days 8, 10, and 12 p.i. **f** Numbers of CD8$^+$ T cells producing IFNγ after incubation of mLN cells (day 12 p.i.) in vitro with or without NP366-374 peptide. **g** Numbers of CD4$^+$ T cells producing IFNγ after incubation of mLN cells (day 12 p.i.) in vitro with or without NP311-325 peptide. Gating of T cells is shown in Fig. S2a. The data are compiled from 1–2 (**a**–**e**) or 4 (**f**–**g**) independent experiments, each with 3–4 animals per WT or KO group. Symbols represent individual mice, with the mean and SD indicated. Significance (**b**–**g**) was evaluated using Mann−Whitney tests, with *p* values indicated

of the CD11b$^+$P1 DC subset and changes in the balance of DC-produced IL-12 and IL-10 in infected KO mice result in decreased numbers of CD8$^+$ MPECs with reduced capacity to complete memory T-cell differentiation.

To determine which DC subset regulates CD8$^+$ Tet$^+$ MPEC numbers, we performed adoptive intranasal transfer of sorted WT CD11b$^+$P1 or CD103$^+$ DC subsets into KO mice, followed immediately by PR8 virus infection. By day 10 p.i., KO mice that received WT CD11b$^+$P1 DCs showed a twofold increase in numbers of MPECs, compared to KO not receiving transferred DCs (Fig. 3g). Transfer of WT CD103$^+$ DCs did not lead to a significant increase in MPECs (Fig. 3g). Numbers of SLECs did not change upon DC transfer (Fig. 3g). These data show that CD11b$^+$P1 DCs preferentially promote MPEC numbers in the primary infection.

Tet$^+$CD8$^+$ T cells in the mLN of KO mice on day 10 p.i. also contained reduced (1.7–2.8-fold) amounts of *Foxo1* and *Klf2* RNA (Fig. 4a). This was consistent with increased (1.6–1.9-fold) amounts

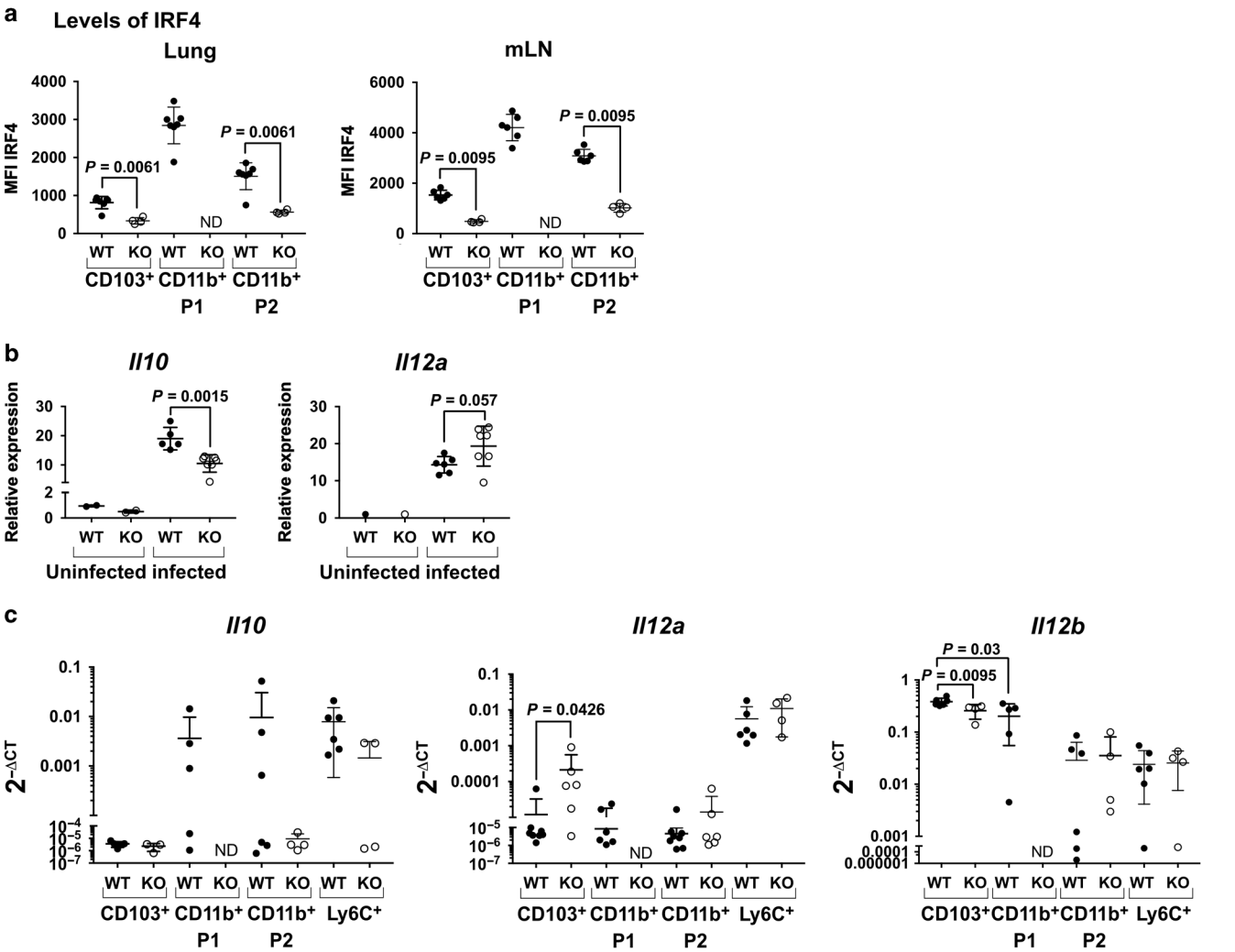

Fig. 2 CD11c$^+$ lung DCs in *CD11c-cre-Irf4$^{f/f}$* mice show decreased *Il10* and increased *Il12a* RNA upon IAV infection. **a** Expression of IRF4 determined by intracellular staining of the indicated DC subsets in lung and mLN of WT and KO mice on day 5 p.i. Gating of DC subsets is shown in Fig. S2b. **b** Relative levels of *Il10* and *Il12a* RNA in total CD11c$^+$ lung cells on days 0 and 3 p.i. determined by qPCR. **c** Levels of *Il10*, *Il12a* and *Il12b* RNA relative to *Gapdh* RNA in sorted lung DC subsets on day 5 p.i. determined by qPCR and compiled from two independent experiments. In all panels, symbols represent individual mice, with the mean and SD indicated. ND, not determined due to absence of the CD11b$^+$P1 subset in KO mice. Significance was evaluated using a *t* test (panel **b**) or one-way ANOVA with a Tukey's multiple comparison test (panels **a**, **c**), with *p* values indicated

of *Il12a* and *Il12b* RNA in the mLN of KO mice on day 8 p.i. (Fig. 4b). Since FOXO1 opposes CD8$^+$ T-cell effector programming and KLF2 regulates LN egress,[38,40] the reduction of *Foxo1* RNA may promote retention of T-cell effectors in the mLN. Indeed, we observed a greater number of Tet$^+$CD8$^+$ T cells in the mLN of KO mice on day 12 p.i. (Fig. 1d).

CD11c-cre-Irf4$^{f/f}$ mice show reduced numbers of CD4$^+$ T regulatory cells in the mLN and lung after infection

IL-10 produced by CD4$^+$ T$_{REGs}$ is required for the transition of MPECs to memory T cells in LCMV infection.[34] Thus, we hypothesized that decreased numbers of induced T$_{REGs}$ may underlie the MPEC defect in KO mice. In homeostasis, the low numbers of CD4$^+$CD25$^+$FOXP3$^+$ T$_{REGs}$ in the mLN and lung did not differ in WT and KO mice (Fig. 5a, b; Fig. S4a). While the numbers of T$_{REGs}$ in the mLN of WT were increased by day 5 p.i., no increase in T$_{REGs}$ was observed in KO mice (16-fold difference) (Fig. 5a). By day 8 p.i., numbers of T$_{REGs}$ in the mLN were comparable in WT and KO mice, suggesting a delay in their differentiation or accumulation in KO mice. Consistent with this, RNA levels of the T$_{REG}$-promoting cytokines *Il10* and *Il2* in the mLN did not differ in WT and KO mice on day 8 p.i. (Fig. 5c). Numbers of T$_{REGs}$ peaked in the lung on day 8 p.i. in WT mice, but notably this expansion was markedly attenuated (1.8-fold) in KO mice and did not occur at later time points (Fig. 5b).

Differentiation of naïve CD4$^+$ T cells to FOXP3$^+$ T$_{REGs}$ is promoted by DC production of IL-10 and TGFβ.[41] To compare the ability of the lung-resident DCs in IAV-infected mice to promote T$_{REG}$ differentiation, we sorted lung DC subsets on day 3 p.i. and incubated them with naïve CD4$^+$CD25$^-$ T cells from OT-II mice (bearing an OVA-specific TCR transgene) and OVA 323–339 peptide. After 6 days, numbers of CD4$^+$CD44$^+$CD25$^+$FOXP3$^+$ T cells were quantified; shown are a compilation of three experiments, in which data were normalized, and the T$_{REG}$ numbers in one representative experiment (Fig. 5d, e; Fig. S4b). WT CD103$^+$ DCs induced T$_{REG}$ differentiation, and this capacity was diminished ~2-fold in KO CD103$^+$ DCs. While WT CD11b$^+$P1 DCs also induced significant T$_{REG}$ numbers, T$_{REG}$ induction by the other CD11b$^+$ DCs (P2 and Ly6C^{hi} iDCs) was minimal. Taken together, these data suggest that both *Irf4* deficiency in CD103$^+$ DCs and the absence of CD11b$^+$P1 DCs decreased T$_{REG}$ differentiation in KO mice during IAV infection.

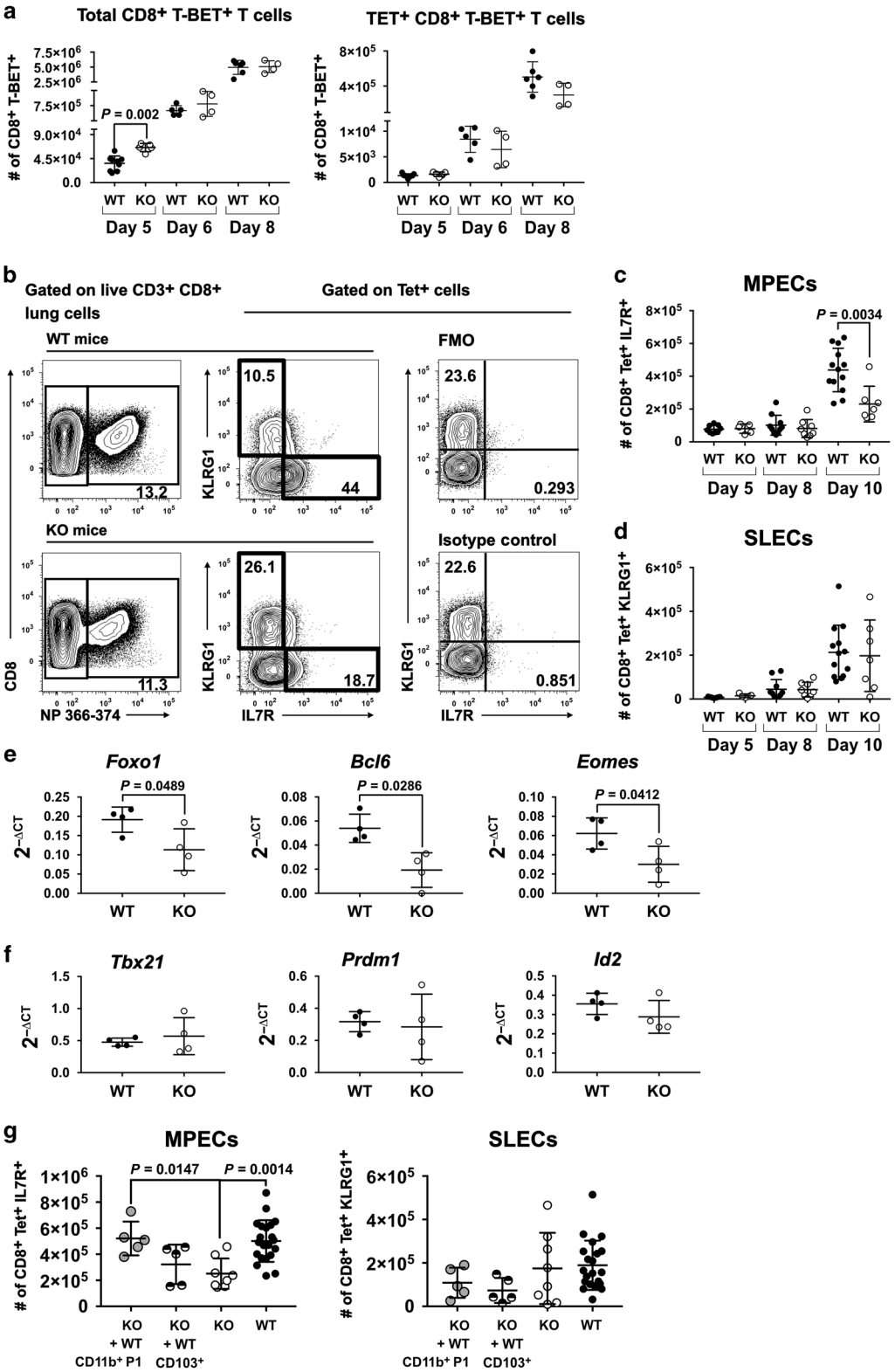

CD11c-cre-Irf4$^{f/f}$ mice recovered from infection show reduced numbers of CD8$^+$ resident memory T-cell populations in the lung In view of the deficit in CD8$^+$ MPECs and CD4$^+$ T_{REGs} in KO mice, we next investigated the T-cell memory populations that remained in the lung and mLN on day 42 p.i. Memory T cells in the lung were identified as extravascular (resident memory, T_{RM}) or vascular (effector memory, T_{EM}) after i.v. injection of a labeled anti-CD45 mAb shortly before euthanasia (Fig. 6a, f; Fig. S5a, b). KO mice showed a threefold reduction in numbers of CD8$^+$Tet$^+$CD69$^+$CD44$^+$CD62L$^-$CD103$^+$ T_{RM}, and a trend to reduced numbers of CD8$^+$Tet$^+$CD69$^+$CD44$^+$CD62L$^-$CD103$^-$ T_{RM} (Fig. 6b–e). Shown are a compilation of two experiments with numbers normalized to the average value in WT mice (Fig. 6b, d) and cell numbers from one representative experiment (Fig. 6c, e).

Fig. 3 *CD11c-cre-Irf4$^{f/f}$* mice show quantitative and qualitative defects in CD8$^+$ memory precursor T cells during the resolution phase of infection. Lung cells were harvested from infected WT and KO mice on days 5, 6, 8, and 10 p.i. Surface and intracellular flow cytometry identified subsets of CD4$^+$ and CD8$^+$ late effector T cells, gated as in Fig. S3b,c. **a** Numbers of CD8$^+$CD44^{hi}T-BET$^+$ and CD8$^+$CD44^{hi}T-BET$^+$ Tet (NP366-374)$^+$ T cells. **b** Gating of Tet(NP366-374)$^+$ CD8$^+$KLRG1$^-$IL-7Rα$^+$ MPECs and CD8$^+$Tet$^+$KLRG1$^+$IL-7Rα$^-$ SLECs. **c** Numbers of MPECs on days 5, 8 and 10 p.i. **d** Numbers of SLECs on days 5, 8, and 10 p.i. **e** Expression of *Foxo1*, *Bcl6* and *Eomes* RNA in CD8$^+$Tet$^+$KLRG1$^-$IL-7Rα$^+$ MPECs sorted on day 10 p.i. determined by qPCR. **f** Expression of *Tbx21*, *Prdm1* and *Id2* genes related to T-cell effector function in MPECs sorted on day 10 p.i. determined by qPCR. Data in panels **a**–**f** are from 1 to 3 independent experiments each with 4–5 animals per WT or KO group. **g** Numbers of MPECs and SLECs on day 10 p.i. after WT CD11b$^+$ P1 or CD103$^+$ DC transfer into KO mice at the time of IAV infection. Data sets showing DC transfer in panel **g** are from three independent experiments, with each experiment involving transfer of either DC subset into 1–2 KO recipients; KO and WT alone data sets include mice analyzed in the DC transfer experiments and the data shown in panels **c** and **d**. In all panels, symbols represent individual mice, with the mean and SD indicated. Significance was evaluated using Mann–Whitney tests (panels **a**, **c**, **d**), unpaired *t* tests (panels **e**, **f**), and one-way ANOVA with Tukey's multiple comparison tests (panel **g**), with *p* values indicated

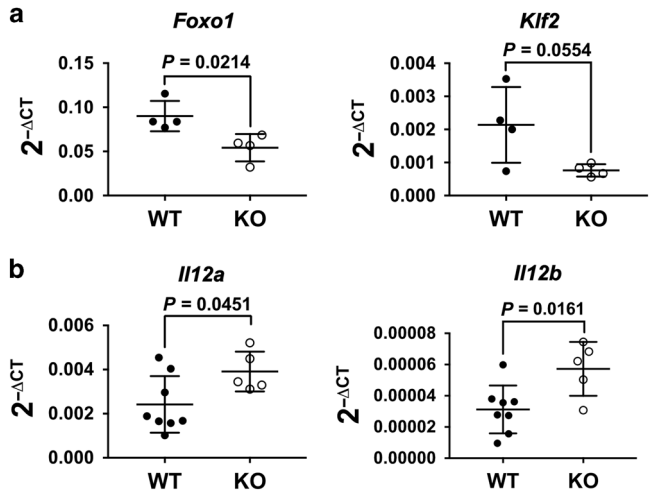

Fig. 4 The mLN of *CD11c-cre-Irf4$^{f/f}$* mice contains elevated *Il12* RNA and antigen-specific CD8$^+$ T cells with reduced expression of *Foxo1* RNA late in infection. **a** CD8$^+$ Tet$^+$ T cells (gated as in Fig. 3b) were sorted from the mLN on day 10 p.i. and assessed for expression of *Foxo1* and *Klf2* RNA by qPCR. **b** Total mLN RNA was assessed for expression of *Il12a* and *Il12b* RNA by qPCR. Symbols represent individual mice, with the mean and SD indicated. Significance was evaluated using unpaired *t* tests, with *p* values indicated

Numbers of CD8$^+$Tet$^+$CD44$^+$CD62L$^-$CD69$^-$CD103$^-$ T_{EM} also were reduced (1.9-fold) in KO mice (Fig. 6g, h; Fig. S5b). In contrast, numbers of CD8$^+$Tet$^+$CD44$^+$CD62L$^+$ T_{CM} in the mLN were not different in WT and KO mice (Fig. 6i–k; Fig. S5c). Numbers of CD4$^+$Tet$^+$ T_{RM}, T_{EM} and T_{CM} did not differ in WT and KO mice (Fig. S5d). Thus, low numbers of MPECs in KO mice at the late stage of infection correlated with reduced numbers of lung CD8$^+$ T_{RM} and T_{EM} in mice fully recovered from infection.

CD11c-cre-Irf4$^{f/f}$ mice have a decreased CD8$^+$ IFNγ$^+$ T-cell response upon secondary infection with a heterosubtypic virus

To determine the functional consequences of the CD8$^+$ T memory defect in KO mice, sequential primary and secondary infections were done with the related X31 (H3N2) and PR8 (H1N1) viruses that share conserved NP T-cell epitopes but differ in the HA and NA proteins that are targets of neutralizing antibodies.[42] WT and KO mice were infected with a sublethal dose of the less virulent X31, and after 42 days, the mice were infected with a lethal dose of the more virulent PR8. During the secondary infection with PR8, the KO mice lost more weight than WT mice, suggesting increased morbidity (Fig. 7a; Fig. S6a). The viral load in WT and KO mice was not different on day 3 p.i. and is not detectable by day 8 p.i. (not shown). On days 3 and 8 p.i., T cells in the mLN and lung were activated ex vivo with the I-A^b-binding NP311-325 and D^b-binding NP366-374 peptides. On day 3 p.i., KO mice showed a significant decrease (~1.9-fold) in the fraction (% of live cells) of NP-specific CD8$^+$ T cells producing IFNγ or TNFα in the mLN (Fig. 7b), but differences in absolute numbers of these cells did not reach statistical significance (Fig. S6b). The amount of IFNγ and TNFα per cell was also decreased 1.5–1.9-fold in KO mice, as judged by MFI (Fig. 7c). In the lung, KO mice showed a 1.9-fold decrease in the fraction (% of live cells) of NP-specific CD8$^+$ T cells producing TNFα (Fig. 7d) and 1.9-fold decreased numbers of antigen-specific CD8$^+$ TNFα$^+$ or IFNγ$^+$ cells (Fig. S6c), but no differences in the amount of IFNγ and TNFα per cell (Fig. 7e). On day 8 p.i. in the mLN, the fraction (% of live cells) of NP-specific CD8$^+$ T cells producing IFNγ, TNFα or IL-2 and the amount of IFNγ per CD8$^+$ T cell also were reduced (1.5–2-fold) in KO mice (Fig. 7f, g), although differences in absolute numbers of these cells did not reach statistical significance (Fig. S6d). In contrast, KO mice showed no difference in the fraction of NP-specific CD4$^+$IFNγ$^+$ T cells in the mLN compared to WT mice on day 3 or day 8 p.i. (Fig. S6e, f). H&E staining of lung tissue sections on day 8 p.i. revealed that while peri-bronchial inflammation was similar in WT and KO mice, the KO mice showed a twofold increase in parenchymal damage characterized by increased alveolar inflammation and thickening of the alveolar wall (Fig. 7h). Extensive lung injury due to viral infection in KO mice is also visible as inflammatory exudate in alveolar spaces and desquamated alveolar epithelial cells upon Periodic Acid-Schiff staining (Fig. S6h).

Similarly, upon primary infection with a sublethal dose of the more virulent PR8 virus followed by secondary infection with X31 virus, KO mice showed decreased numbers of antigen-specific CD8$^+$IFNγ$^+$ and CD8$^+$IL-2$^+$ T cells but no difference in the numbers of antigen-specific CD4$^+$IFNγ$^+$ T cells compared to WT mice (Fig. S6g). These data show that defects in the CD8$^+$ T_{RM} and T_{EM} subsets after a primary influenza infection in KO mice led to a weaker CD8$^+$ T-cell effector response upon infection with a heterosubtypic virus, correlating with increased morbidity and lung pathology.

DISCUSSION

In the context of a heterogeneous CD11b$^+$ population encompassing lung-resident DCs and iDCs, the role of the resident CD11b$^+$CD24^{hi} DC subset in effector and memory T-cell differentiation during IAV infection remained unclear. To address this, we used *CD11c-cre-Irf4$^{f/f}$* (KO) mice bearing *Irf4* deficiency in CD11c$^+$ cells, which in homeostasis lack the IRF4-dependent lung-resident CD11b$^+$CD24^{hi} P1 DCs, while CD11b$^+$CD24^{int} P2 and CD103$^+$ DC subsets are present in normal numbers but lack IRF4.[6] In a sublethal IAV infection, these DC defects resulted in increased numbers of IFNγ$^+$CD8$^+$ T-cell effectors yet reduced numbers of MPECs. The remaining MPECs in KO mice expressed lower levels of *Foxo1* and its downstream targets *Bcl6* and *Eomes* important for solidification of the memory CD8$^+$ T-cell transcriptional program. These quantitative and qualitative defects in the MPEC population led to decreased numbers of CD8$^+$ T_{RM} and T_{EM} cells in the memory T-cell pool of recovered mice. Upon infection with a heterosubtypic IAV, NP-specific CD8$^+$ T-cell effector responses were significantly reduced in the KO mice and correlated with

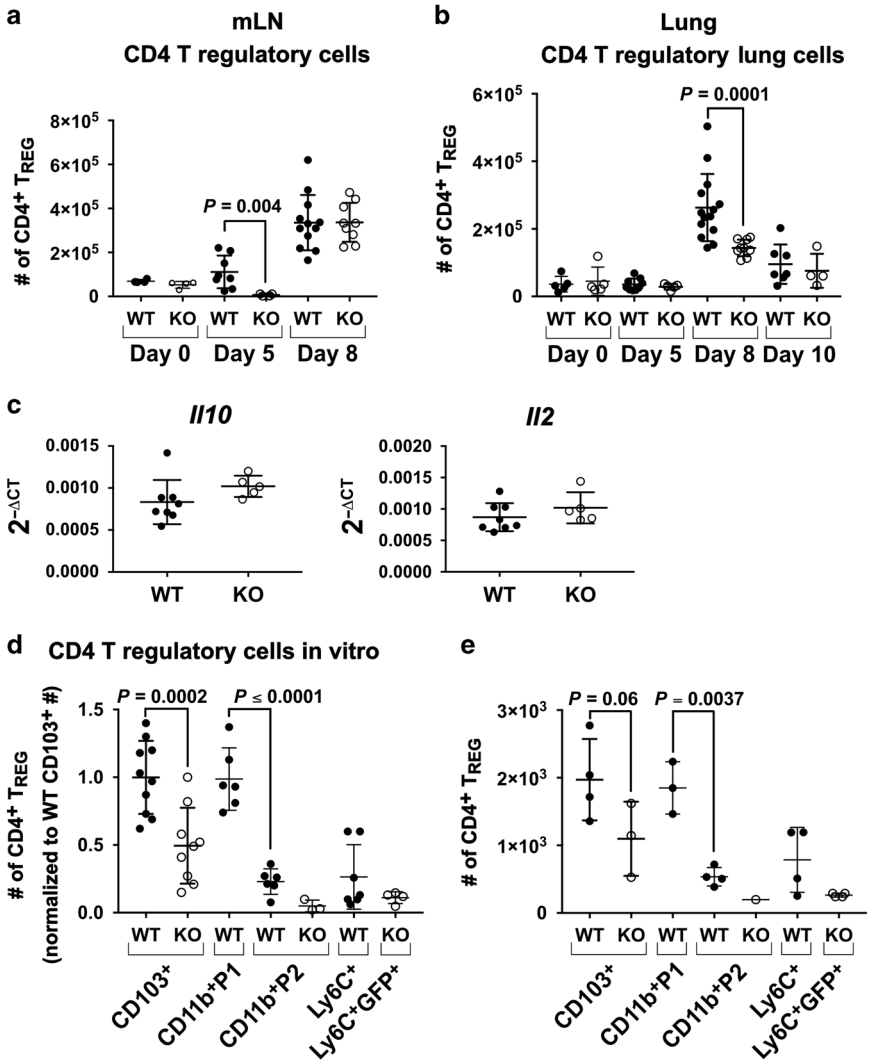

Fig. 5 *CD11c-cre-Irf4*$^{f/f}$ mice show reduced numbers of CD4$^+$ FOXP3$^+$ T_{REGs} in the mLN and lung after IAV infection. **a**, **b** Lung and mLN cells were harvested from infected mice on days 0, 5, 8, and 10 p.i. Surface and intracellular staining identified T_{REGs} (Fig. S2a). Shown are numbers of CD4$^+$CD25$^+$FOXP3$^+$ T_{REGs} in the **a** mLN and **b** lung. **c** Expression of *Il10* and *Il2* RNA in total mLN cells on day 8 p.i. determined by qPCR. **d** Numbers of FOXP3$^+$ T_{REGs} in cultures normalized to the average of WT CD103$^+$ DCs (gated as in Fig. S4b) after in vitro incubation of naïve CD4$^+$ OT-II T cells with OVA323-339 peptide and isolated lung DC subsets (1000 per well) sorted on day 3 p.i. **e** Numbers of FOXP3$^+$ T_{REGs} in cultures from one representative experiment. Symbols represent individual mice, with the mean and SD indicated. The data are compiled from 1 to 3 independent experiments each with 3–5 animals per WT or KO group. Significance was evaluated using a Mann−Whitney test (panels **a**–**c**) or one-way ANOVA with Tukey's multiple comparison test (panels **d**, **e**), with *p* values indicated

increased lung parenchyma pathology consistent with injury caused by viral infection. Thus during IAV infection, IRF4-expressing DCs act to attenuate the CD8$^+$ T-cell effector response while promoting a population of IAV-specific CD8$^+$ memory precursor cells that ultimately leads to a robust population of tissue-localized T_{RM} and circulating T_{EM} cells.

While the molecular mechanisms of memory T-cell differentiation have been well defined,[32,33] our understanding of the possibly distinct roles of DC subsets in CD8$^+$ memory T-cell differentiation during IAV infection was incomplete. Early cross-presentation of viral antigens by CD103$^+$ DCs is important for priming of T_{RM}, but CD103$^+$ DCs are dispensable for full T_{RM} differentiation or generation of circulating memory T cells.[30] The role of CD11b$^+$P1 DC responses in IAV infection were previously queried with different *CD11c-cre-Irf4*$^{f/f}$ mice bearing a "late-acting" CD11c-cre that does not delete *Irf4* in pre-cDCs, leaving normal numbers of the CD11b$^+$P1 subset in KO mice.[21] These KO mice did not show any differences in the fraction of IAV-specific CD4$^+$ or CD8$^+$ IFNγ or TNFα T cells on day 8 p.i. This suggested that IRF4 expression in CD11b$^+$P1 and other lung cDCs was not required for IAV-specific T-cell responses. However, differentiation of effector CD8$^+$ T-cell subsets (SLECs and MPECs) and memory responses were not investigated, so it is difficult to compare their findings to work in our model in which an "early-acting" CD11c-cre leads to the absence of the CD11b$^+$P1 DCs as well as IRF4 deficiency in CD103$^+$ DCs. Because the major difference between the two lines of *CD11c-cre-Irf4*$^{f/f}$ mice is the absence of CD11b$^+$P1 DCs, we hypothesized that these DCs promote CD8$^+$ memory T cells. To determine if either the CD11b$^+$P1 or CD103$^+$ DCs preferentially promote MPECs, we transferred sorted WT lung DC subsets into KO mice at the time of infection. Importantly, transfer of WT CD11b$^+$P1 DCs, but not CD103$^+$ DCs, into KO mice led to increased numbers of MPECs on day 10 p.i. T_{REG} numbers in the lung have waned at this time point, so it was not possible to determine if the CD11b$^+$P1 or CD103$^+$ DCs promote T_{REG} differentiation in these experiments. These data support our hypothesis that the absence of the CD11b$^+$P1 DCs is the primary driver of the CD8$^+$ T memory defect in *CD11c-cre-Irf4*$^{f/f}$ mice. This

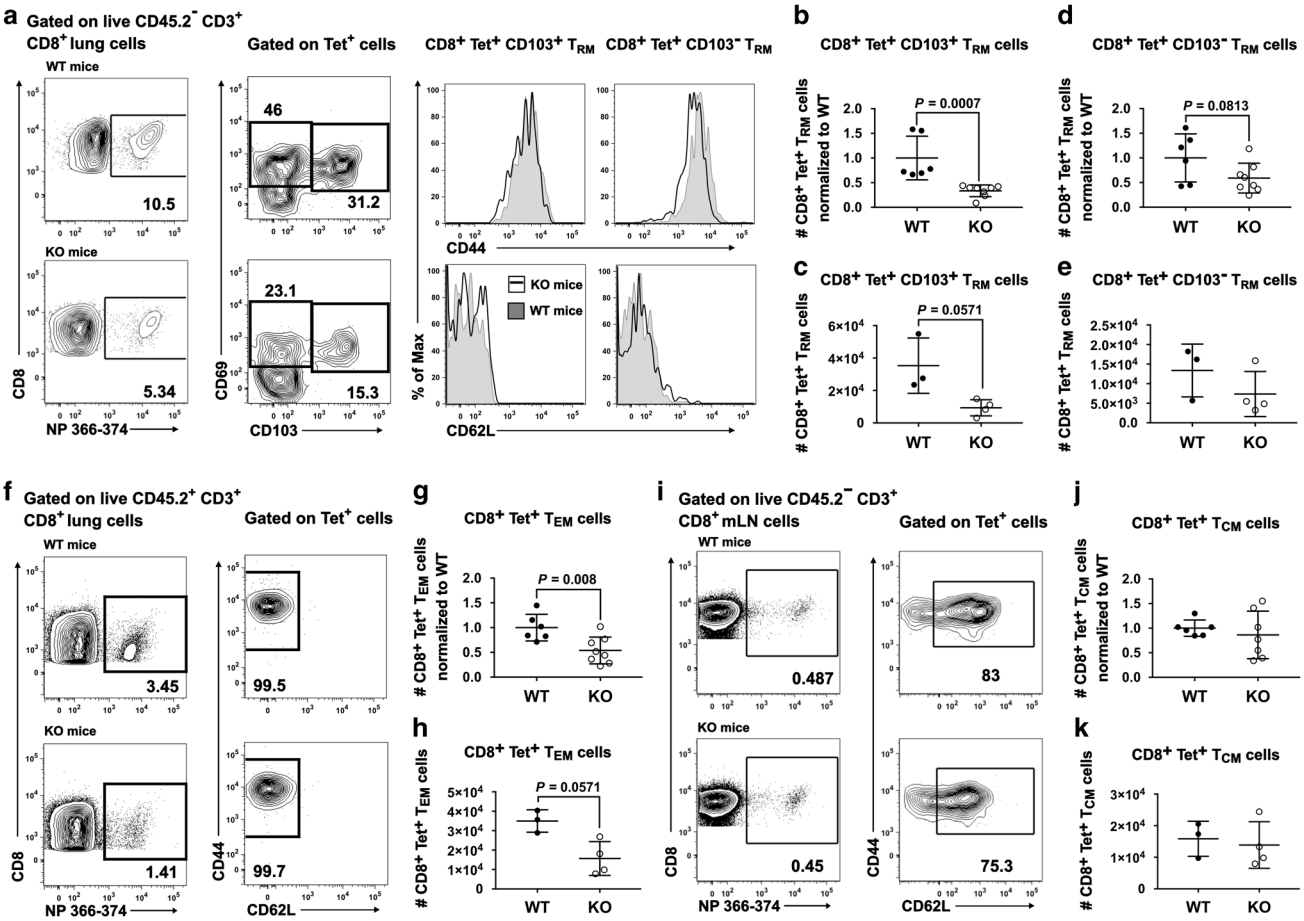

Fig. 6 *CD11c-cre-Irf4$^{f/f}$* mice recovered from primary IAV infection show reduced numbers of CD8$^+$ T_{RM} and T_{EM} populations in the lung. On day 42 p.i., CD45.2$^+$ cells in blood were marked by i.v. injection of an α-CD45 mAb before euthanasia and identification of memory T-cell subsets using flow cytometry (Fig. S5). **a** Gating of extravascular (i.v. CD45$^-$) CD8$^+$Tet$^+$CD69^{hi}CD44^{hi}CD62L$^-$CD103$^+$ or CD103$^-$ T_{RM} cells in the lung. **b** Numbers of CD8$^+$Tet$^+$CD69^{hi}CD44^{hi}CD62L$^-$CD103$^+$ T_{RM} normalized to the average of WT mice. **c** Numbers of CD8$^+$Tet$^+$CD69^{hi}CD44^{hi}CD62L$^-$CD103$^+$ T_{RM} cells from one representative experiment. **d** Numbers of CD8$^+$Tet$^+$CD69^{hi}CD44^{hi}CD62L^{-i}CD103$^-$ T_{RM} normalized to the average of WT mice. **e** Numbers of CD8$^+$Tet$^+$CD69^{hi}CD44^{hi}CD62L$^-$CD103$^-$ T_{RM} cells from one representative experiment. **f** Gating of vascular (i.v. CD45$^+$) CD8$^+$Tet$^+$CD62L$^-$CD44$^+$ T_{EM} cells. **g** Numbers of CD8$^+$Tet$^+$CD44$^+$CD62L$^-$CD69$^-$CD103$^-$ T_{EM} normalized to the average of WT mice. **h** Numbers of CD8$^+$Tet$^+$CD44$^+$CD62L$^-$CD69$^-$CD103$^-$ T_{EM} cells from one representative experiment. **i** Gating of CD8$^+$Tet$^+$CD62L$^+$CD44$^+$ T_{CM} in the mLN. **j** Numbers of CD8$^+$Tet$^+$CD62L$^+$CD44$^+$ T_{CM} normalized to the average of WT mice. **k** Numbers of CD8$^+$Tet$^+$CD62L$^+$CD44$^+$ T_{CM} from one representative experiment. Symbols represent individual mice, with the mean and SD indicated. Normalized data are compiled from two independent experiments with 3–4 animals per WT and KO group. Significance was evaluated using a Mann−Whitney test, with *p* values indicated

finding also is consistent with the above-mentioned study showing that CD103$^+$ DCs are not required for complete T_{RM} differentiation.[30]

Our data suggest that CD11b$^+$P1 DCs regulate both the lung T_{RM} and T_{EM} pools by promoting expression of *Foxo1*, *Bcl6* and *Eomes* in MPECs, thus ensuring their complete differentiation and/or maintenance. Notably, FOXO1 opposes CD8$^+$ T-cell effector programming while instructing early memory T-cell fate, and *Foxo1*-deficient mice contain fewer memory T cells and more CD8$^+$ T-cell effectors,[38,39,43] comparable to our results with KO mice. Continuous FOXO1 activity also is required to maintain the memory state of CD8$^+$ T cells,[43,44] suggesting that the reduced *Foxo1* levels in memory T cells in KO mice may be insufficient to maintain the memory state. Levels of FOXO1 in differentiating memory CD8$^+$ T cells are regulated by the balance of IL-10 and IL-12 in the local environment. IL-10R signaling acts via PI3K-AKT to block the phosphorylation of FOXO1, thus inhibiting its degradation and allowing nuclear translocation and transcription of downstream genes such as *Bcl6*.[45] In contrast, IL-12R signaling acting via AKT promotes the phosphorylation and degradation of FOXO1, thus increasing T-BET expression.[38] Thus, our data suggest that the deficit of IL-10 and excess of IL-12 in the absence of the IRF4-dependent CD11b$^+$P1 DCs leads to reduced FOXO1 expression in differentiating memory T cells.

Our finding is consistent with a report showing that the absence of IL-10 leads to decreased *Foxo1* in maturing memory CD8$^+$ T cells in LCMV infection and that T_{REGs} are a significant source of IL-10 promoting MPEC differentiation.[34] IAV infection also results in a significant population of antigen-specific T_{REGs},[36] and we observed a marked deficit of FOXP3$^+$ T_{REGs} in lungs of KO mice on day 8 p.i. This suggests that IL-10-producing IRF4-dependent DCs first promote T_{REG} differentiation, and the T_{REGs} in turn produce the IL-10 needed for MPEC differentiation. Alternately or in parallel, DCs producing IL-10 or displaying other cytokines such as TGFβ or IL-15 may directly promote MPEC differentiation and/or maintenance of memory T-cell populations.[33] Our in vitro assays showed that both CD103$^+$ and CD11b$^+$P1 DCs promoted differentiation of naïve CD4$^+$ T cells into FOXP3$^+$ T_{REGs}. Our DC transfer experiments did not permit assessment of T_{REGs} because their numbers in the lung have waned by day 10 p.i., the optimal

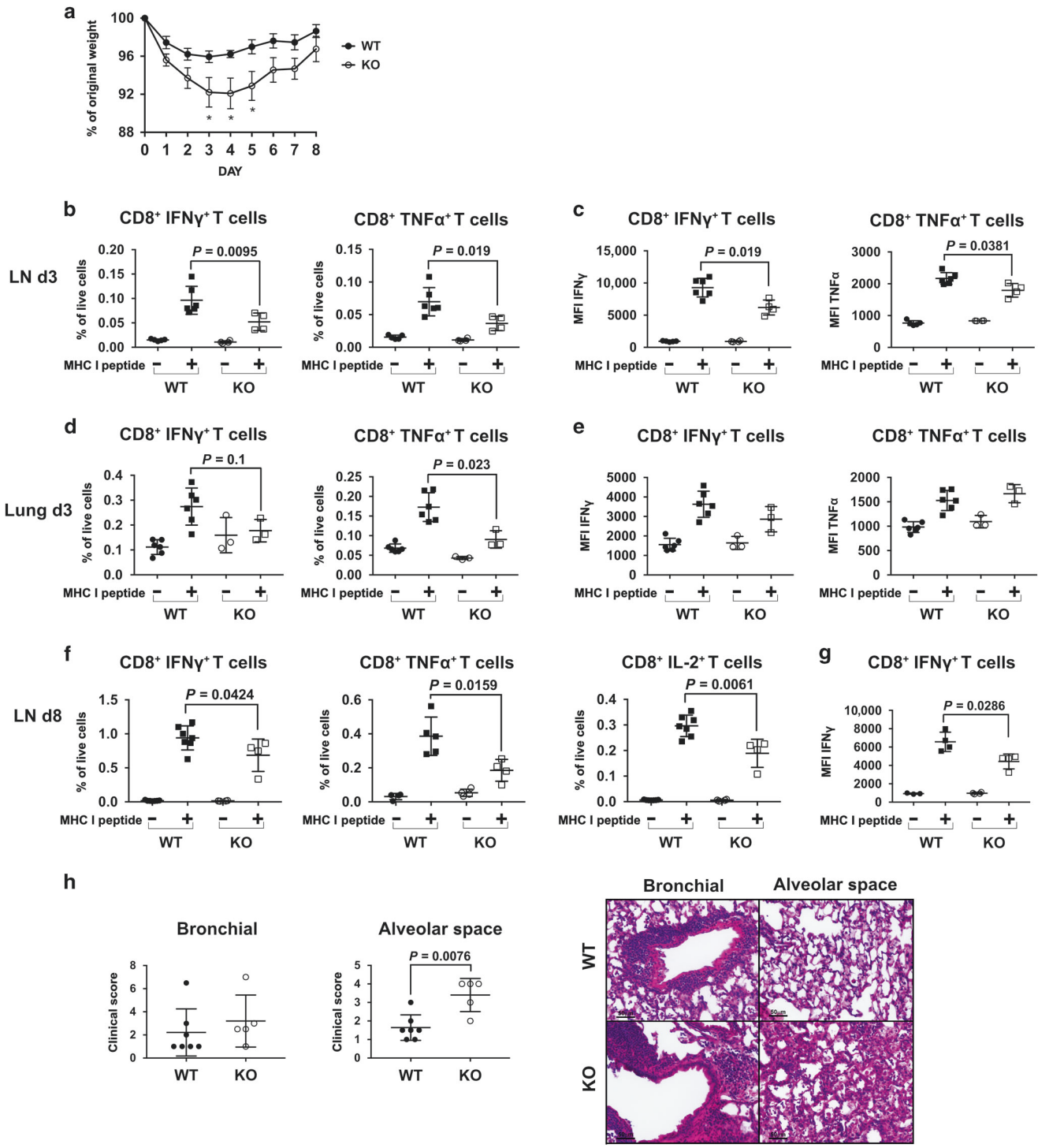

Fig. 7 *CD11c-cre-Irf4$^{f/f}$* mice show a decreased CD8$^+$ effector T-cell response upon secondary infection with a heterosubtypic IAV. WT and KO mice were infected with X31 virus and then infected with a lethal dose of PR8 virus 41 days later. **a** Weight loss over 8 days p.i. Shown are the mean and SEM, $n = 5–7$. Data were analyzed using a multiple *t* test with the Bonferroni−Sidak method. Significant results (*) correspond to an adjusted $p < 0.05$. **b** On day 3 p.i., the fraction (frequency of live cells) of CD8$^+$ T cells producing IFNγ or TNFα (gated as in Fig. S2a) after incubation of mLN cells in vitro with or without NP366-374 peptide. **c** The MFI of IFNγ or TNFα expression in NP-specific mLN T cells on day 3 p.i. **d** On day 3 p.i., the fraction (frequency of live cells) of CD8$^+$ T cells producing IFNγ or TNFα after incubation of lung cells in vitro with or without NP366-374 peptide. **e** The MFI of IFNγ or TNFα expression in NP-specific lung T cells on day 3 p.i. **f** On day 8 p.i., the fraction (frequency of live cells) of CD8$^+$ T cells producing IFNγ, TNFα or IL-2 after incubation of mLN cells in vitro with or without NP366-374 peptide. **g** The MFI of IFNγ expression in NP-specific mLN T cells on day 8 p.i. **h** Lung sections (day 8 p.i.) stained with H&E were scored for inflammation and tissue damage in the bronchial and alveolar space. In panels **b**−**h**, symbols represent individual mice, with the mean and SD indicated. The data shown are from one of two independent experiments with 4–6 animals each per WT and KO group. Significance was evaluated using Mann−Whitney tests, with *p* values indicated

time point for MPEC assessment. KO CD103$^+$ DCs were less capable of inducing T_{REG} differentiation, raising the possibility that *Irf4* deficiency alters the ability of CD103$^+$ DCs to produce mediators such as active TGFβ that promotes *Foxp3* expression during T_{REG} generation.[46] Preliminary comparisons of WT and KO CD103$^+$ DCs did not reveal significant differences in expression of genes in pathways important for T_{REG} generation, including *Tgfb1*, *Tgfb2, Tgfb3, Lrrc32, Itgb8, Ahr*, *Aldhla2*, *Entpd1*, *Ebi3*, or *Il27* (IH, manuscript in preparation). Thus, the absence of CD11b$^+$P1 DCs producing IL-10 and a defect in CD103$^+$ DCs may contribute to the paucity of T_{REGs} in the KO lung.

Dysregulation of one or more pathways may explain the increased numbers of NP-specific CD8$^+$ and CD4$^+$ T cells capable of producing IFNγ in the mLN after resolution of infection in KO mice. TCR and IL-12R signaling determine the levels of T-BET and the terminal differentiation of IL-7R^{lo} SLECs,[31] and elevated IL-12 in KO mice was associated with increased numbers of T-BET$^+$ T cells on day 5 p.i., perhaps indicative of increased effector differentiation. However, numbers of antigen-specific T-BET$^+$ cells and SLECs were equivalent in lungs of WT and KO mice at later time points, suggesting that KO mice may instead have a defect in effector contraction or egress of antigen-specific T cells from the mLN. Consistent with this, NP-specific CD8$^+$ T cells in the mLN of KO mice contained reduced *Foxo1* and *Klf2* RNA on day 10 p.i. FOXO1 regulates *Klf2*, which promotes expression of $S1P_1$ and CD62L that are important for naïve T-cell recirculation, and *Klf2* deficiency results in retention of naïve T cells in LNs.[40] Thus, antigen-specific CD4$^+$ and CD8$^+$ T cells may accumulate in the mLN of KO mice due to a reduced ability to egress from the LN.

The increased numbers of antigen-specific CD8$^+$ and CD4$^+$ T cells by day 12 p.i. in KO mice was associated with reduced numbers of CD8$^+$ but not CD4$^+$ memory cells, suggesting that signals from CD11b$^+$P1 DCs are less important for specification of the CD4$^+$ memory T-cell program. CD4$^+$ memory T-cell formation and lung homing during IAV infection requires viral antigen and costimulatory molecule recognition at later stages of infection during the peak of effector generation.[47,48] At days 6–8 p.i., iDCs and CD11b$^+$P2 DCs predominate in the lung and their antigen presentation, costimulation and cytokine production may promote the formation and retention of CD4$^+$ T_{RM} cells. The absence of a defect in CD4$^+$ memory T cells in KO mice may reflect our finding that Ly6C$^+$ iDCs and CD11b$^+$P2 DCs are present in comparable numbers in lungs of WT and KO mice (IH, manuscript in preparation). These CD11b$^+$ subsets accumulating later in infection in mLN also may support our finding that CD8$^+$ T_{CM} cells do not differ in WT and KO mice, consistent with the observation that prolonged antigen presentation promotes CD8$^+$ T-cell memory programming during IAV infection.[19,49] Similarly, iDCs were required for the persistence but not differentiation of circulating and lung-resident CD8$^+$ memory T cells in respiratory poxvirus infection.[50]

Upon secondary infection with a heterosubtypic virus bearing conserved NP epitopes, KO mice mounted a weaker antiviral CD8$^+$ T-cell response, characterized by reduced numbers of NP-specific CD8$^+$ T cells capable of making IFNγ, TNFα or IL-2, and reduced levels of IFNγ and TNFα in responding T cells. This is consistent with quantitative and qualitative deficits in the T_{RM} and T_{EM} compartments, but the response is not entirely abolished perhaps due to an intact T_{CM} pool. Recent work shows that DCs are not absolutely required for the initial response of T_{RMs} during secondary infection, although they likely contribute to the strength of the recall response.[51–53] Our data show early defects in the CD8$^+$ T memory cell program during the primary infection of KO mice, but we cannot rule out a role for IRF4-dependent DCs in the maintenance or reactivation of T_{RM} populations in the lung.

In contrast to nonlymphoid tissues such as skin and the female reproductive tract, numbers of IAV-specific T_{RM} in the lower respiratory tract wane over time, leading to loss of heterosubtypic immunity.[24,27] Recent work showed that the gradual loss of T_{RMs} is due to an imbalance of their apoptosis and replacement through conversion of circulating T_{EMs}.[26] Since IRF4-dependent CD11b$^+$P1 DCs regulate the differentiation of the T_{RM} and T_{EM} pools, vaccination strategies that target this subset of lung-resident DCs during primary and booster immunizations may maximize the retention of respiratory tract CD8$^+$ T_{RM} cells.

METHODS

Mice

Mice (purchased from The Jackson Laboratory) bearing a conditional allele of *Irf4* (B6.129S1-Irf4<tm1Rdf>/J)[54] were bred to mice bearing Cre recombinase driven by the CD11c promoter (B6.Cg-Tg(Itgax-cre)1–1Reiz/J)[55] and then interbred to yield *CD11c-cre-Irf4$^{f/f}$* or *CD11c-cre-Irf4$^{+/+}$* mice. Upon deletion of the *Irf4* allele, an *Egfp* minigene is placed in frame such that *Irf4$^{-/-}$* cells are GFP$^+$. Mice used as "wild- type" were either Cre$^+$ but bearing two WT alleles of *Irf4*, or Cre$^-$ and bearing either WT or conditional *Irf4* alleles. The Cre activity may randomly act in CD11c$^-$ cells in the line of CD11c-Cre mice, leading to mice that have the conditional allele deleted in many tissues.[6] Therefore, we screened for global deletion of *Irf4* using PCR primers (forward: 5′-CAGGATGTTGCCGTCCTCCTTG-3′ and reverse: 5′-CCTGCAGCCAA-TAAGCTTATAAC-3′), and excluded those mice from this study. Littermate mice of each genotype and both sexes were analyzed at 10–12 weeks of age. OT-II mice bearing a transgenic TCR specific for I-A^b/OVA323-339 (B6.Cg-Tg(TcraTcrb)425Cbn/J) were purchased from The Jackson Laboratory. The Oklahoma Medical Research Foundation Institutional Animal Care and Use Committee approved the studies.

Influenza virus infection

Viruses were grown in embryonated chicken eggs, and viral end point titer (egg infectious units, EIU) was determined using allantoic fluid in a hemagglutination assay in the lab of Dr. Gillian Air (Oklahoma University Health Sciences Center). HA genes were sequenced to confirm identity of virus stocks. Mice were infected intranasally with 30 µl PBS containing 5×10^2 EIU of mouse adapted A/Puerto Rico/8/1934 (PR8, H1N1) virus. For sequential infections with heterosubtypic viruses, mice were initially infected with A/X31 (H3N2) virus (3×10^5 EIU), which carries the HA and NA genes of A/Hong Kong/1/1968 (H3N2) on the PR8 background, and then secondarily infected with 2×10^4 EIU of PR8 on day 42 post infection. Alternately, mice initially infected with PR8 were infected on day 42 post infection with 3×10^5 EIU of X31 virus. Mice were weighed each day to track morbidity during the infection.

Isolation of cells from tissues

Lungs were perfused with PBS + 1 mM EDTA before digestion for 45–60 min with collagenase type A (1 mg/ml) or Liberase (0.1 mg/ml) and DNase I (0.1 mg/ml) (all from Roche) in PBS + 0.5% BSA pH 7.4. Mediastinal lymph nodes (mLN) were mechanically disrupted into single-cell suspension. Lung and LN cells were filtered (40 µM), washed with RPMI + 10% FCS or HBSS without Ca^{2+} and Mg^{2+}, respectively, and red cells lysed using RBC lysis buffer (BD Biosciences). To distinguish populations of T cells present in lung tissue or blood, a fluorochrome-labeled anti-CD45 mAb was injected into the intra-orbital vein shortly before mice were euthanized.[56]

Ex vivo T-cell stimulation

$3–4 \times 10^6$ mLN cells were incubated with the H-2D^b-binding NP366-374 peptide (2 µg/ml) (MBLI) and the I-A^b-binding NP311-325 peptide (2 µg/ml) (Bio-Synthesis Inc) and brefeldin A (5 µg/ml) (BD Biosciences) in RPMI + 5%FCS for 5 h. Surface and intracellular

staining identified IFNγ, TNFα or IL-2 producing $CD4^+$ and $CD8^+$ T cells.

Flow cytometry
For surface staining, cells were incubated with mAbs on ice for 15 min after 5 min of anti-CD16/32 treatment in FACS buffer (PBS, 5% newborn calf serum, 0.1% NaN_3). Kits for intranuclear staining (ThermoFisher Scientific) and intracellular cytokine staining (BD Biosciences) were used according to the manufacturer's instructions. T cells were identified with fluorochrome-linked mAbs specific for CD45.2-APCCy7 (104), CD3-PECy7 (145-2C11), CD4-BV786 (GK1.5), CD8α-APCfire750 and -APC (53–6.7), IL7Rα-BIO (A7R34), KLRG1-BV421(2F1/KLRG1), CD44-BV711 (1M7), T-BET-PEDazzle (4B10), CD25-PerCPCy5.5 (PC61), CD103-BV711(2E7), FOXP3-PE (MF-14), CD62L-PerCPCy5.5 (MEL-14), CD69-BV605 (H1.2F3), IFNγ-PE (XMG1.2), IL-2-PEDazzle (JES6-5H4), TNFα-BV711 (MP6-XT22). DC subsets were identified with mAbs specific for CD11c-PECy7 (N418), CD103-BV711 (M290), CD11b-BV786 (M1/70), SIGLECF-APCCy7 (E20-2240), MHCII-AF700 (M5/114.15.2), SIRPα-PEDazzle (P8), CD24-PerCpCy5.5 (M1/69), Ly6C-BV605 (HK 1.4), CD88-APC (20/70), CD26-PE (H194-11), IRF4-PE (3E4). mAbs were purchased from BD Biosciences, Biolegend, Tonbo Biosciences, and ThermoFisher Scientific. Tetramers of H-$2D^b$-NP366-374-PE were purchased from MBL International. Tetramers of I-A^b-NP311-325-APC and negative control I-A^b-PVSKMRMATPLLMQA-APC were obtained from the NIH Tetramer Core Facility. Live/dead cell discrimination was done with a fixable zombie aqua dye (Biolegend). Samples were acquired on an LSRII instrument containing four lasers (BD Biosciences) and analyzed using FlowJo software (Treestar).

Cell sorting
$CD11c^+$ cells were enriched from collagenase/DNAse-digested lungs on days 0 or 3 p.i. using a CD11c positive selection magnetic bead kit (StemCell Technologies). To sort lung DC subsets on day 5 p.i., DCs within a lung digest were enriched by gradient separation with OptiPrep (Axis-Shield) according to the manufacturer's protocol. DC subsets were identified and sorted after staining with mAbs to DC surface markers listed above as in Fig. S2b. In KO mice, *Irf4*-deficient DCs were sorted as GFP^+, since not all $Ly6C^+$ iDCs were GFP^+. Tet^+CD8^+ MPECs (GFP^-) in lung and $CD8^+$ T cells in the mLN were sorted on day 10 p.i. after enrichment on a 40% Percoll gradient and staining with mAbs specific for CD3-PECy7 (145-2C11), CD8α-APC or APCfire750 (53-6.7), IL7Rα-BIO (A7R34), KLRG1-BV421 (2F1/KLRG1), Streptavidin BV605 and H-$2D^b$- NP366-374-PE tetramer as in Fig. 3. T-cell and DC subsets were sorted directly into ARCTURUS PicoPure RNA extraction buffer (ThermoFisher Scientific) using a BD FACS Aria II instrument.

Adoptive transfer of DCs
$CD11b^+$ P1 and $CD103^+$ DC subsets were sorted from lungs of naïve WT mice (pools of 15–18 mice) as described above. Each sort yielded enough DCs for 1–2 recipients of each DC subset. 8×10^4 $CD11b^+$ P1 or $CD103^+$ DCs were transferred intranasally into KO mice, followed by infection with 30 µl PBS containing 5×10^2 EIU of mouse adapted A/Puerto Rico/8/1934 (PR8, H1N1) virus. The mice were analyzed for numbers of lung $CD8^+$ MPECs on day 10 p.i.

T regulatory cell assays
Lung DC subsets were sorted on day 3 p.i. (as in Fig. S2b) and 1000 DCs incubated in complete RPMI + 5% FCS with 100 nM OVA323-339 peptide (InvivoGen) and 20,000 naïve $CD4^+CD25^-$ T cells isolated from OT-II spleens using a naïve $CD4^+$ T cell isolation kit (Biolegend). Recombinant IL-2 (5 ng/ml, Peprotech) was added after 2 days. After 6 days, numbers of $CD4^+CD44^+CD25^+FOXP3^+$ T cells were quantified using flow cytometry.

Isolation of RNA and real-time quantitative PCR
RNA of sorted immune cells was isolated with a PicoPure™ RNA Isolation Kit and amplified with an Ovation Pico SL WTA System V2 kit (NuGEN). Quantitative real-time RT-PCR (qPCR) of genes was performed with iTaq™ Universal SyBr® Green Supermix or iTaq™ Universal Probes Supermix (Bio-Rad) on an ABI 7900HT instrument. Expression of tested genes relative to *Gapdh* expression was determined using the $2^{-\Delta Ct}$ method. The primers are listed in supplementary Table 1.

Histologic analyses
The medium lung lobe was inflated and fixed with 10% neutral buffered formalin (Sigma-Aldrich) and embedded in paraffin. Lung sections (5 µM thickness) were stained with hematoxylin and eosin (H&E) or Periodic Acid-Schiff stain. Images were acquired using a Zeiss Axioplan Microscope, with a ×20 objective. Lung pathology was evaluated for severity of peri-bronchial inflammation, and bronchial epithelial cell and goblet cell hyperplasia and epithelial shedding or necrosis. Each criterion was scored on a scale of 0−4 with 0 = no involvement and 1–4 representing increasing severity. The results are represented as a cumulative bronchial score. Extent of inflammation in the parenchyma with hyperplasia or thickening of the alveolar wall was also assessed and the results are presented as alveolar space pathology. All slides were read by an observer blinded to experimental details.

Cytokine assays
Bronchoalveolar lavage (BAL) fluid was collected by washing the lung cavity with PBS three times using an intratracheal catheter (Tom cat 3.5 Fr ×5.5″, Santa Cruz Animal Health). IFNγ in the BAL fluid was measured using xMAP multiplex assays in the OMRF Serum Analyte and Biomarker core facility. ProcartaPlex kits (ThermoFisher Scientific) were used according to the manufacturer's instructions.

Viral RNA detection
Lung cells were lysed with Trizol reagent (Ambion), and RNA was isolated with a Trizol-RNeasy® mini kit (QIAGEN) hybrid protocol. cDNA was synthesized using iScript™ gDNA Clear cDNA Synthesis kit (BIO-RAD). qPCR was performed with iTaq™ Universal Probes Supermix (BIO-RAD) using a FAM-labeled probe 5′-CTCAGTTATT CTGCTGGTGCACTTGCCA-3′, PCR forward primer 5′-GGACTGCAG CGTAGACGCTT-3′ and reverse primer 5′-CATCCTGTTGTATATGAG GCCCAT-3′ targeting the gene encoding the influenza M1 protein on an ABI 7900HT instrument.[57] Relative expression of the gene was determined using the ΔΔCt method with normalization to *Gapdh* expression.

Statistical analyses
Comparison between two groups was performed using a two-tailed Mann−Whitney or Student's *t* test. A one-way ANOVA with a Tukey's post test was performed for multiple comparisons. Weight loss curves were analyzed by a multiple *t* test using the Bonferroni−Sidak method. The differences were considered significant with a p value < 0.05. Prism 7 software was used for all analyses.

ACKNOWLEDGEMENTS
We thank Dr. Gillian Air and Shelly Gulati at OUHSC for assistance with growing and titering virus in eggs, Dr. Diana Hamilton and Jacob Bass in the OMRF Flow Cytometry Core Facility, and the staff of the Comparative Medicine Facility. This work was supported by NIH HL119501 (to S. Kovats) and by an OMRF Patricia and Don Capra Predoctoral Fellowship (to S. Kadel).

AUTHOR CONTRIBUTIONS

E.A.-E. designed and performed experiments, analyzed data and wrote the manuscript. I.H. and H.B. designed and performed experiments and analyzed data. S. Kadel, S.T., J.P. and S.S. performed experiments. S. Kovats conceived of the study, designed experiments, analyzed data and wrote the manuscript.

ADDITIONAL INFORMATION

The online version of this article (https://doi.org/10.1038/s41385-019-0173-1) contains supplementary material, which is available to authorized users.

Competing interests: The authors declare no competing interests.

Publisher's note: Springer Nature remains neutral with regard to jurisdictional claims in published maps and institutional affiliations.

REFERENCES

1. Braciale, T. J., Sun, J. & Kim, T. S. Regulating the adaptive immune response to respiratory virus infection. *Nat. Rev. Immunol.* **12**, 295–305 (2012).
2. Moskophidis, D. & Kioussis, D. Contribution of virus-specific CD8 + cytotoxic T cells to virus clearance or pathologic manifestations of influenza virus infection in a T cell receptor transgenic mouse model. *J. Exp. Med* **188**, 223–232 (1998).
3. Krammer, F. et al. Influenza. *Nat. Rev. Dis. Prim.* **4**, 3 (2018).
4. Zens, K. D., Chen, J. K. & Farber, D. L. Vaccine-generated lung tissue-resident memory T cells provide heterosubtypic protection to influenza infection. *JCI Insight* **1**, e85832 (2016).
5. Wakim, L. M., Smith, J., Caminschi, I., Lahoud, M. H. & Villadangos, J. A. Antibody-targeted vaccination to lung dendritic cells generates tissue-resident memory CD8 T cells that are highly protective against influenza virus infection. *Mucosal Immunol.* **8**, 1060–1071 (2015).
6. Bajaña, S., Turner, S., Paul, J., Ainsua-Enrich, E. & Kovats, S. IRF4 and IRF8 act in CD11c+ cells to regulate terminal differentiation of lung tissue dendritic cells. *J. Immunol.* **196**, 1666–1677 (2016).
7. Schlitzer, A. et al. IRF4 transcription factor-dependent CD11b+ dendritic cells in human and mouse control mucosal IL-17 cytokine responses. *Immunity* **38**, 970–983 (2013).
8. Edelson, B. T. et al. Peripheral CD103+ dendritic cells form a unified subset developmentally related to CD8alpha+ conventional dendritic cells. *J. Exp. Med.* **207**, 823–836 (2010).
9. Ginhoux, F. et al. The origin and development of nonlymphoid tissue CD103+ DCs. *J. Exp. Med.* **206**, 3115–3130 (2009).
10. Haniffa, M. et al. Human tissues contain CD141hi cross-presenting dendritic cells with functional homology to mouse CD103+ nonlymphoid dendritic cells. *Immunity* **37**, 60–73 (2012).
11. Nakano, H. et al. Blood-derived inflammatory dendritic cells in lymph nodes stimulate acute T helper type 1 immune responses. *Nat. Immunol.* **10**, 394–402 (2009).
12. Aldridge, J. R. J. et al. TNF/iNOS-producing dendritic cells are the necessary evil of lethal influenza virus infection. *Proc. Natl Acad. Sci. USA* **106**, 5306–5311 (2009).
13. Kim, T. S. & Braciale, T. J. Respiratory dendritic cell subsets differ in their capacity to support the induction of virus-specific cytotoxic CD8+ T cell responses. *PLoS ONE* **4**, e4204 (2009).
14. GeurtsvanKessel, C. H. et al. Clearance of influenza virus from the lung depends on migratory langerin+ CD11b- but not plasmacytoid dendritic cells. *J. Exp. Med.* **205**, 1621–1634 (2008).
15. Ballesteros-Tato, A., Leon, B., Lund, F. E. & Randall, T. D. Temporal changes in dendritic cell subsets, cross-priming and costimulation via CD70 control CD8(+) T cell responses to influenza. *Nat. Immunol.* **11**, 216–224 (2010).
16. Ho, A. W. et al. Lung CD103+ dendritic cells efficiently transport influenza virus to the lymph node and load viral antigen onto MHC class I for presentation to CD8 T cells. *J. Immunol.* **187**, 6011–6021 (2011).
17. Helft, J. et al. Cross-presenting CD103+ dendritic cells are protected from influenza virus infection. *J. Clin. Invest.* **122**, 4037–4047 (2012).
18. Krishnaswamy, J. K. et al. Migratory $CD11b^+$ conventional dendritic cells induce T follicular helper cell-dependent antibody responses. *Sci. Immunol.* **2**, pii: eaam9169 (2017).
19. Kim, T. S., Gorski, S. A., Hahn, S., Murphy, K. M. & Braciale, T. J. Distinct dendritic cell subsets dictate the fate decision between effector and memory CD8(+) T cell differentiation by a CD24-dependent mechanism. *Immunity* **40**, 400–413 (2014).
20. Martínez-López, M., Iborra, S., Conde-Garrosa, R. & Sancho, D. Batf3-dependent CD103+ dendritic cells are major producers of IL-12 that drive local Th1 immunity against Leishmania major infection in mice. *Eur. J. Immunol.* **45**, 119–129 (2015).
21. Williams, J. W. et al. Transcription factor IRF4 drives dendritic cells to promote Th2 differentiation. *Nat. Commun.* **4**, 2990 (2013).
22. Rosato, P. C., Beura, L. K. & Masopust, D. Tissue resident memory T cells and viral immunity. *Curr. Opin. Virol.* **22**, 44–50 (2017).
23. Gebhardt, T., Mueller, S. N., Heath, W. R. & Carbone, F. R. Peripheral tissue surveillance and residency by memory T cells. *Trends Immunol.* **34**, 27–32 (2013).
24. Wu, T. et al. Lung-resident memory CD8 T cells (TRM) are indispensable for optimal cross-protection against pulmonary virus infection. *J. Leukoc. Biol.* **95**, 215–224 (2014).
25. McMaster, S. R., Wilson, J. J., Wang, H. & Kohlmeier, J. E. Airway-resident memory CD8 T cells provide antigen-specific protection against respiratory virus challenge through rapid IFN-γ production. *J. Immunol.* **195**, 203–209 (2015).
26. Slütter, B. et al. Dynamics of influenza-induced lung-resident memory T cells underlie waning heterosubtypic immunity. *Sci. Immunol.* **2**, pii: eaag2031 (2017).
27. Shane, H. L., Reagin, K. L. & Klonowski, K. D. The respiratory environment diverts the development of antiviral memory CD8 T cells. *J. Immunol.* **200**, 3752–3761 (2018).
28. Purwar, R. et al. Resident memory T cells (T(RM)) are abundant in human lung: diversity, function, and antigen specificity. *PLoS ONE* **6**, e16245 (2011).
29. Kumar, B. V. et al. Human tissue-resident memory T cells are defined by core transcriptional and functional signatures in lymphoid and mucosal sites. *Cell Rep.* **20**, 2921–2934 (2017).
30. Iborra, S. et al. Optimal generation of tissue-resident but not circulating memory T cells during viral infection requires crosspriming by $DNGR\text{-}1^+$ dendritic cells. *Immunity* **45**, 847–860 (2016).
31. Kaech, S. M. & Cui, W. Transcriptional control of effector and memory CD8+ T cell differentiation. *Nat. Rev. Immunol.* **12**, 749–761 (2012).
32. Chang, J. T., Wherry, E. J. & Goldrath, A. W. Molecular regulation of effector and memory T cell differentiation. *Nat. Immunol.* **15**, 1104–1115 (2014).
33. Mackay, L. K. & Kallies, A. Transcriptional regulation of tissue-resident lymphocytes. *Trends Immunol.* **38**, 94–103 (2017).
34. Laidlaw, B. J. et al. Production of IL-10 by CD4(+) regulatory T cells during the resolution of infection promotes the maturation of memory CD8(+) T cells. *Nat. Immunol.* **16**, 871–879 (2015).
35. Croom, H. A. et al. Memory precursor phenotype of CD8+ T cells reflects early antigenic experience rather than memory numbers in a model of localized acute influenza infection. *Eur. J. Immunol.* **41**, 682–693 (2011).
36. Betts, R. J. et al. Influenza A virus infection results in a robust, antigen-responsive, and widely disseminated Foxp3+ regulatory T cell response. *J. Virol.* **86**, 2817–2825 (2012).
37. Akbari, M. et al. IRF4 in dendritic cells inhibits IL-12 production and controls Th1 immune responses against Leishmania major. *J. Immunol.* **192**, 2271–2279 (2014).
38. Rao, R. R., Li, Q., Gubbels Bupp, M. R. & Shrikant, P. A. Transcription factor Foxo1 represses T-bet-mediated effector functions and promotes memory CD8(+) T cell differentiation. *Immunity* **36**, 374–387 (2012).
39. Hess Michelini, R., Doedens, A. L., Goldrath, A. W. & Hedrick, S. M. Differentiation of CD8 memory T cells depends on Foxo1. *J. Exp. Med.* **210**, 1189–1200 (2013).
40. Carlson, C. M. et al. Kruppel-like factor 2 regulates thymocyte and T-cell migration. *Nature* **442**, 299–302 (2006).
41. Li, M. O. & Flavell, R. A. Contextual regulation of inflammation: a duet by transforming growth factor-beta and interleukin-10. *Immunity* **28**, 468–476 (2008).
42. Kreijtz, J. H. et al. Primary influenza A virus infection induces cross-protective immunity against a lethal infection with a heterosubtypic virus strain in mice. *Vaccine* **25**, 612–620 (2007).
43. Tejera, M. M., Kim, E. H., Sullivan, J. A., Plisch, E. H. & Suresh, M. FoxO1 controls effector-to-memory transition and maintenance of functional CD8 T cell memory. *J. Immunol.* **191**, 187–199 (2013).
44. Delpoux, A. et al. Continuous activity of Foxo1 is required to prevent anergy and maintain the memory state of $CD8^+$ T cells. *J. Exp. Med.* **215**, 575–594 (2018).
45. Kim, E. H. & Suresh, M. Role of PI3K/Akt signaling in memory CD8 T cell differentiation. *Front. Immunol.* **4**, 20 (2013).
46. Chen, W. et al. Conversion of peripheral CD4+ CD25- naive T cells to CD4+ CD25+ regulatory T cells by TGF-beta induction of transcription factor Foxp3. *J. Exp. Med.* **198**, 1875–1886 (2003).
47. Jelley-Gibbs, D. M. et al. Unexpected prolonged presentation of influenza antigens promotes CD4 T cell memory generation. *J. Exp. Med.* **202**, 697–706 (2005).
48. Chang, Y. H. et al. Dichotomous expression of TNF superfamily ligands on antigen-presenting cells controls post-priming anti-viral $CD4^+$ T cell immunity. *Immunity* **47**, 943–958.e9 (2017).
49. León, B., Ballesteros-Tato, A., Randall, T. D. & Lund, F. E. Prolonged antigen presentation by immune complex-binding dendritic cells programs the proliferative capacity of memory CD8 T cells. *J. Exp. Med.* **211**, 1637–1655 (2014).

50. Desai, P., Tahiliani, V., Stanfield, J., Abboud, G. & Salek-Ardakani, S. Inflammatory monocytes contribute to the persistence of CXCR3^{hi} CX3CR1^{lo} circulating and lung-resident memory CD8$^+$ T cells following respiratory virus infection. *Immunol. Cell Biol.* **96**, 370–378 (2018).
51. Shin, H., Kumamoto, Y., Gopinath, S. & Iwasaki, A. CD301b+ dendritic cells stimulate tissue-resident memory CD8+ T cells to protect against genital HSV-2. *Nat. Commun.* **7**, 13346 (2016).
52. Park, S. L. et al. Local proliferation maintains a stable pool of tissue-resident memory T cells after antiviral recall responses. *Nat. Immunol.* **19**, 183–191 (2018).
53. Beura, L. K. et al. Intravital mucosal imaging of CD8$^+$ resident memory T cells shows tissue-autonomous recall responses that amplify secondary memory. *Nat. Immunol.* **19**, 173–182 (2018).
54. Klein, U. et al. Transcription factor IRF4 controls plasma cell differentiation and class-switch recombination. *Nat. Immunol.* **7**, 773–782 (2006).
55. Caton, M. L., Smith-Raska, M. R. & Reizis, B. Notch-RBP-J signaling controls the homeostasis of CD8- dendritic cells in the spleen. *J. Exp. Med*. **204**, 1653–1664 (2007).
56. Anderson, K. G. et al. Intravascular staining for discrimination of vascular and tissue leukocytes. *Nat. Protoc.* **9**, 209–222 (2014).
57. Crowe, C. R. et al. Critical role of IL-17RA in immunopathology of influenza infection. *J. Immunol.* **183**, 5301–5310 (2009).